IEEE Access
Multidisciplinary | Rapid Review | Open Access Journal

Received May 19, 2021, accepted August 20, 2021, date of publication August 27, 2021, date of current version September 3, 2021.

Digital Object Identifier 10.1109/ACCESS.2021.3108488

A New Electromechanical Analogy Approach Based on Electrostatic Coupling for Vertical Dynamic Analysis of Planar Vehicle Models

JAVIER LÓPEZ-MARTÍNEZ[1], JAVIER CASTILLO MARTÍNEZ[1], DANIEL GARCÍA-VALLEJO[2], ALFREDO ALCAYDE[1], AND FRANCISCO G. MONTOYA[1]

[1]CIAIMBITAL Research Centre, ceiA3, Department of Engineering, University of Almería, 04120 Almería, Spain
[2]Department of Mechanical Engineering and Manufacturing, Universidad de Sevilla, 41092 Seville, Spain

Corresponding author: Francisco G. Montoya (pagilm@ual.es)

This work was supported in part by Spanish Ministry of Science, Innovation, and Universities at the University of Almeria through the Program "Proyectos de I+D de Generacion de Conocimiento" of the National Program for the Generation of Scientific and Technological Knowledge and Strengthening of the R+D+I System under Grant PGC2018-098813-B-C33.

ABSTRACT Analogies between mechanical and electrical systems have been developed and applied for almost a century, and they have proved their usefulness in the study of mechanical and electrical systems. The development of new elements such as the inerter or the memristor is a clear example. However, new applications and possibilities of using these analogues remain to be explored. In this work, the electrical analogues of different vehicle models are presented. A new and not previously reported analogy between inertial coupling and electrostatic capacitive coupling is found and described. Several examples are provided to highlight the benefits of this analogy. Well-known mechanical systems like the half-car or three three-axle vehicle models are discussed and some numerical results are presented. To the best of the author's knowledge, such systems were never dealt with by using a full electromechanical analogy. The mechanical equations are also derived and compared with those of the electrical domain for harmonic steady-state analysis.

INDEX TERMS Electromechanical analogy, capacitive coupling, vertical dynamics, vehicle model.

I. INTRODUCTION

Analogies can be established between different physical domains, such as mechanical, electrical, fluid, or thermal systems since they are modeled with comparable differential equations. Dynamical analogies are based on energy relations. In [1], Jeltsema & Scherpen provided an overview of both the energy- and power-based modeling frameworks in different physical domains and discuss their mutual relationships.

The mechanical-electrical analogy was developed and rather extensively used in 30-40's of the 20th century for the study of vibrations in linear mechanical systems [2]–[6], where the use of mechanical to electrical analogy was empowered by the existing solution methods for electrical networks. One of the earlier works that solved a mechanical system using electrical network theory was written by Harrison [7] in a patent of an invention published in 1929. A detailed overview with interesting historical notes of the conception and evolution of electromechanical analogy can be found in the work of Gardonio and Brennan [8].

Two different analogues have been used to translate mechanical systems into electrical ones. Historically, the first proposed analogy related force to voltage. In this so-called "force-voltage" analogy [3] (also known as "direct analogy"), the mechanical mass is related with an electrical inductor and the mechanical spring with an electrical capacitor. Few years after this analogy had been adopted, some difficulties or limitations were pointed out in [2] since the physical interpretation of the electric network analogue was not direct from the mechanical system. In the force-voltage analogy, the relationship between mechanical and electrical elements does not preserve the same topology, i.e. mechanical elements arranged in series (parallel) are represented by electrical elements arranged in parallel (series). Moreover, the concept of *through* and *across* variables are inverted. A *through* variable is measured on a single point of an element, as performed with force and current measures, while

The associate editor coordinating the review of this manuscript and approving it for publication was Chaitanya U. Kshirsagar.

the value of an *across* variable is obtained as the difference between the measurements in two different points, such as the case of velocity and voltage [6]. Then, in the force-voltage analogy, a force being a *through* variable in the mechanical system corresponds to a voltage, which is an *across* variable in the electrical system.

To overcome these constraints, a new ''force-current'' analogy was formulated [2], [9], and the concept of *bar impedance* (later on renamed as *mobility*) was introduced [10]. This alternative analogy, also known as ''inverse analogy'', preserves the same topology for both mechanical and electrical systems, while keeping the equivalence between *through* and *across* variables.

Despite the above, any of the described analogies are mathematically valid and may be applied indistinctly. Furthermore, depending on the specific mechanical problem, one analogy may be more appropriate over the other and easier to derive [4], [8]. In other cases, it could be even necessary to use both analogies to draw different parts of a mechanical system. The different electric diagrams derived are then linked using appropriate couplers [11]. It should be noted that the two possible electric analogues obtained for a given mechanical system (force-voltage and force-current) are dual to each other. Then, it is possible to transform one into another following some basic relations [4]. As in the electric network, the duality principle holds for mechanical systems [12]. Some illustrative examples of dual mechanical systems can be found in [13].

Beyond purely mechanical systems, the utility of analogues is especially remarkable when mechanical systems are linked to electrical systems. In this multidomain problem, the mechanical system is replaced by its electrical equivalent and joined to the electrical one. In this way, a unique electrical system is studied [14], [15]. de Silva [16] proposed the use of linear graphs for modeling multi-domain systems in a unified way, thus allowing to exploit the existing analogies across domains. More recently, de Silva [17] introduced a systematic approach for modeling multi-domain systems in a ''unique'' (single) model having physically meaningful variables, and many illustrative examples were described.

Mechanical systems can be directly drawn as mechanical ''circuit'' or diagrams using mechanical symbols, instead of using an electrical representation, but where the electric principles can be applied. This approach is known as the ''mobility method'' when the same topology of the mechanical system is preserved (as in the force-current analogy), or the ''impedance method'' when the topology is changed as in the force-voltage analogy [10], [13]. Firestone [10] stated the equivalent of Kirchhoff's laws for the mobility method: (i) Force Law: the sum of all forces acting on any junction point is zero; (ii) Velocity Law: the sum of all the velocities across the structures included in any closed mechanical circuit is zero. The solutions of these mechanical diagrams are then obtained without any reference to electric systems [18].

Working with analogues facilitates the transfer of knowledge and ideas between different branches of science and engineering. It motivates scientists to become interested in other fields, to create synergies and interdisciplinary working groups. Also, in the educational field, the use of analogues helps in approaching and understanding the different subjects [19]. Analogues allow solving the problems of one physical system by using resolution methods of another physical system that may show some advantage. In this sense, it has been more often preferred to work with electrical analogues, while there are interesting works where the mechanical analogue of electrical power systems was used, see references [20], [21] and [22].

Analogies between different physical domains have helped in finding new elements. This is the case of the memristor. In the electrical domain, a memristor is a two-terminal circuit element characterized by a relationship between the charge and the flux linkage. The existence of that missing constitutive relation was described by Chua in 1971 [23], though it was not until 2008 when an electrical passive memristive device was constructed [24]. One year after the work of Chua, Oster & Auslander [25] proposed a tapered dashpot as a mechanical memristor, showing a relation between displacement and momentum, which are the mechanical analogues of electric charge and flux linkage. Another remarkable contribution attributable to the use of analogues is the invention of the inerter [26]. The inerter was the result of searching for a genuine two-terminal mechanical device equivalent to the electrical capacitor. Unlike a conventional mass element, the electrical equivalent of the inerter does not require a grounded terminal. The inerter is the true dual of the spring and it has been successfully applied to suspension vehicles [27], [28].

Electro-mechanical analogies have been used in vehicle suspension modeling and control [29]–[32], in vehicle drive trains [33], in structural dynamics [34], in modeling and control of flexible structures [35], in design and optimization of inductive power transfer systems [36], and in piezoelectric vibration energy harvesters [37], among others mechanical or electromechanical systems with interest in vibrations [14], [15], [38]–[42].

The present work is a contribution to the use of electromechanical analogues in vehicle suspensions. To the authors' knowledge, the use of electrical analogues in the scientific literature regarding vehicle suspension is limited to the quarter-car model. In this work, the full electromechanical analogue of a half-car vehicle model, where the inertial coupling appears due to the vehicle mainframe, is presented. The relationship between mechanical inertial coupling and electrostatic capacitor coupling is then described. This is a novelty of this work in the quest of identifying new analogies. Furthermore, the analogy is extended to a three-axle vehicle model in which some numerical results are obtained and discussed.

II. ELECTRICAL ANALOGIES OF MECHANICAL SYSTEMS. A BASIC EXAMPLE

The process followed to obtain an electric analogy of a mechanical system is shown in this section with the help of the 2 d.o.f translational model depicted in figure 1. Masses m_1 and m_2 are linked by a spring and a damper arranged in parallel, with k_2 and d_2 as stiffness and damping constants, respectively. Mass m_1 is connected to the ground by another parallel spring-damper pair with stiffness and damping constants k_1 and d_1, respectively. An external force $f(t)$ is acting on the mass m_2. Using the mobility method [13], figure 1b shows the mechanical network of the model, where masses m_1 and m_2 are "connected" to the ground due to the inertial frame of reference, i.e., the velocity and acceleration of these masses are measured relative to ground.

The equations of motion of the system in figure 1a can be obtained by using Lagrange equations [43] in terms of the independent variables x_1 and x_2, which are the components of the generalized co-ordinates vector $\boldsymbol{x} = [x_1 \;\; x_2]^T$ as follows:

$$\frac{d}{dt}\left(\frac{\partial L}{\partial \dot{\boldsymbol{x}}}\right) - \frac{\partial L}{\partial \boldsymbol{x}} + \frac{\partial F_R}{\partial \dot{\boldsymbol{x}}} = \boldsymbol{Q}_a(t) \tag{1}$$

where $L = T - \Pi$ is the lagrangian function, T is the kinetic energy, Π is the potential energy, F_R is a Rayleigh dissipation function, and $\boldsymbol{Q}_a(t)$ is the generalized applied force vector. The expressions of T, Π and F_R are read as follows:

$$T = \frac{1}{2}m_1\dot{x}_1^2 + \frac{1}{2}m_2\dot{x}_2^2 \tag{2}$$

$$\Pi = \frac{1}{2}k_1x_1^2 + \frac{1}{2}k_2\,(x_2 - x_1)^2 \tag{3}$$

$$F_R = \frac{1}{2}d_1\dot{x}_1^2 + \frac{1}{2}d_2\,(\dot{x}_2 - \dot{x}_1)^2 \tag{4}$$

Introducing T, Π, F_R and $\boldsymbol{Q}_a(t) = [0 \;\; -f(t)]^T$ into Eq. (1), the following ODE system is found:

$$\underbrace{\begin{bmatrix} m_1 & 0 \\ 0 & m_2 \end{bmatrix}}_{\boldsymbol{m}}\underbrace{\begin{bmatrix} \ddot{x}_1 \\ \ddot{x}_2 \end{bmatrix}}_{\ddot{\boldsymbol{x}}} + \underbrace{\begin{bmatrix} d_1 + d_2 & -d_2 \\ -d_2 & d_2 \end{bmatrix}}_{\boldsymbol{d}}\underbrace{\begin{bmatrix} \dot{x}_1 \\ \dot{x}_2 \end{bmatrix}}_{\dot{\boldsymbol{x}}} + \underbrace{\begin{bmatrix} k_1 + k_2 & -k_2 \\ -k_2 & k_2 \end{bmatrix}}_{\boldsymbol{k}}\underbrace{\begin{bmatrix} x_1 \\ x_2 \end{bmatrix}}_{\boldsymbol{x}} = \underbrace{\begin{bmatrix} 0 \\ -f(t) \end{bmatrix}}_{\boldsymbol{Q}(t)} \tag{5}$$

which may be rewritten in matrix form as

$$\boldsymbol{m}\ddot{\boldsymbol{x}} + \boldsymbol{d}\dot{\boldsymbol{x}} + \boldsymbol{k}\boldsymbol{x} = \boldsymbol{Q}(t) \tag{6}$$

Note that $\boldsymbol{Q}(t) = \boldsymbol{Q}_a(t)$ in (6), but this is not always the case, as it will be shown for vehicle models subject to excitations coming from the road profile.

This mechanical system can be studied through any of the two well-known versions of electromechanical analogies. Table 1 summarizes the relationship between the electrical and mechanical elements and variables for the force-voltage and force-current analogies. Both electrical analogues are shown in figure 2, where some basic connection rules have been followed [4]. Mainly, when the force-voltage analogy is used, parallel (series) connections in the mechanical systems must be drawn as series (parallel) connections in the electrical network. Conversely, if the force-current analogy is preferred, the topology of the diagrams is not altered [6]. The latter is a very strong argument in favor of the force-current analogy. Furthermore, it will also facilitate the resolution of the proposed networks. Therefore, the force-current version will be used in the rest of this work.

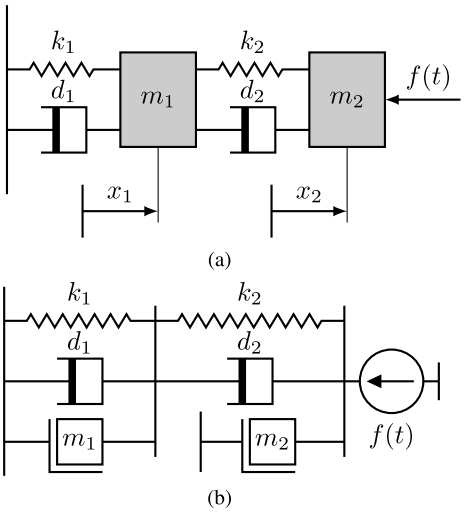

FIGURE 1. (a) 2 d.o.f. mechanical model and (b) its network representation.

Figure 2b represents the force-current analogue of the mechanical system of figure 1. It can be seen that the topology of the electrical circuit is identical to the mechanical one. It is worth mentioning that capacitors must always have a lead to the common node or earth. As explained before, a mass that moves with respect to the ground (the inertial frame), behaves like a capacitor tied to the ground in the electrical network.

Note that once the topology of the electrical analogue is found, it can be used for either time or frequency domain analysis. Based on table 1 and the use of Kirchhoff's current law (KCL), the following equation can be obtained:

$$\boldsymbol{C}\ddot{\boldsymbol{\phi}} + \boldsymbol{G}\dot{\boldsymbol{\phi}} + \boldsymbol{B}\boldsymbol{\phi} = \boldsymbol{I}(t) \tag{7}$$

which can be expanded to:

$$\begin{bmatrix} C_1 & 0 \\ 0 & C_2 \end{bmatrix}\begin{bmatrix} \ddot{\phi}_1 \\ \ddot{\phi}_2 \end{bmatrix} + \begin{bmatrix} G_1 + G_2 & -G_2 \\ -G_2 & G_2 \end{bmatrix}\begin{bmatrix} \dot{\phi}_1 \\ \dot{\phi}_2 \end{bmatrix} + \begin{bmatrix} B_1 + B_2 & -B_2 \\ -B_2 & B_2 \end{bmatrix}\begin{bmatrix} \phi_1 \\ \phi_2 \end{bmatrix} = \begin{bmatrix} 0 \\ -i_2(t) \end{bmatrix} \tag{8}$$

where $G_i = \frac{1}{R_i}$ is the conductance of resistor R_i and $B_i = \frac{1}{L_i}$ is the inverse of inductance L_i. The variable ϕ is the flux linkage. Note that $\dot{\phi}_j = u_j$ is the voltage of node j and the force $f(t)$ has been replaced by its analogue $i(t)$. It can be readily observed that (7) and (8) are similar to (6) and (5), respectively. For steady state harmonic analysis, Eq. (8) can be transferred to the frequency domain by using the Euler expression, where a sine or cosine can be put in

TABLE 1. General analogy between mechanical and electrical systems.

Mechanical variables		Electrical system analogy			
		Force-voltage		Force-current	
Force [N]	F	u	Voltage [V]	i	Current [A]
Velocity [m/s]	v	i	Current [A]	u	Voltage [V]
Spring [N/m]	k	$C = 1/k$	Capacitor [F]	$L = 1/k$	Inductor [H]
Mass (inerter) [kg]	m	$L = m$	Inductor [H]	$C = m$	Capacitor [F]
Damper [Ns/m]	d	$R = d$	Resistor [Ω]	$R = 1/d$	Resistor [Ω]

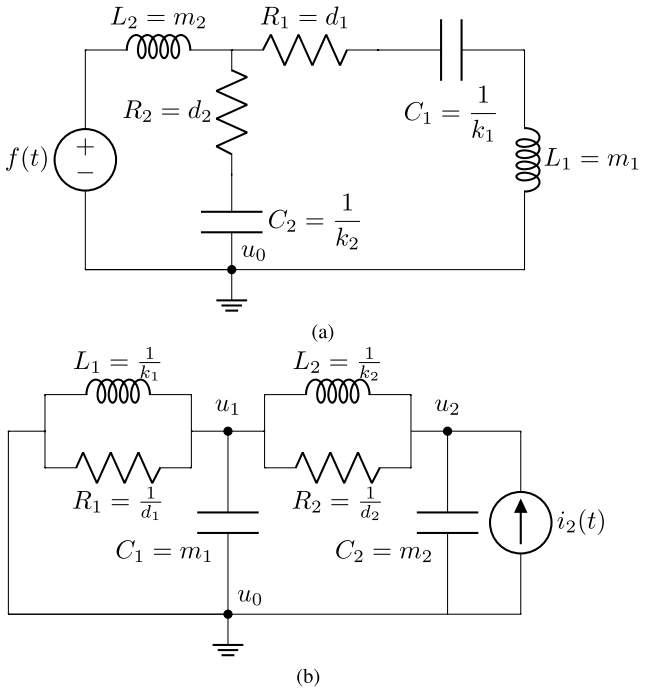

FIGURE 2. (a) Force-voltage and (b) force-current analogues of the 2 d.o.f. mechanical model of figure 1.

complex form. For example,

$$\begin{aligned} e(t) &= \sqrt{2}E\cos(\omega t+\varphi) \\ &= Re\{\sqrt{2}\cos(\omega t+\varphi)+j\sqrt{2}E\sin(\omega t+\varphi)\} \\ &= Re\{\sqrt{2}Ee^{j\omega t+\varphi}\} = Re\{\sqrt{2}\vec{E}e^{j\omega t}\} \end{aligned} \tag{9}$$

where $\vec{E} = Ee^{j\varphi}$ is known as a phasor. It indicates the RMS (E) and phase (φ) value of the harmonic sinusoid, respectively. This transformation allows a complete rewriting of sinusoidal time domain equations in a complex linear algebraic. Thus, Eq. (8) can be written in a compact way as follows:

$$\begin{bmatrix} 0 \\ \vec{I}_2 \end{bmatrix} = \underbrace{\begin{bmatrix} G_1+\vec{B}_{L_1}+\vec{B}_{C_1}+G_2+\vec{B}_{L_2} & -G_2-\vec{B}_{L_2} \\ -G_2-\vec{B}_{L_2} & \vec{B}_{C_2}+G_2+\vec{B}_{L_2} \end{bmatrix}}_{\vec{Y}} \times \underbrace{\begin{bmatrix} \vec{U}_1 \\ \vec{U}_2 \end{bmatrix}}_{\vec{U}} \tag{10}$$

where $\vec{B}_{L_i} = \frac{1}{L_i\omega j}$ is the susceptance (inverse of complex reactance) associated to L_i and $\vec{B}_{C_i} = C_i\omega j$ is the susceptance associated to C_i. The matrix system in (10) is composed of complex numbers and can be easily solved by using matrix linear algebra. The unknown voltages $\vec{U}_1$ and $\vec{U}_2$ are obtained by inverting the admittance matrix $[\vec{Y}]$:

$$[\vec{U}] = [\vec{Y}]^{-1}[\vec{I}] \tag{11}$$

Once the voltages are known, every current can be solved by applying Ohm's law to any element of the circuit. This is equivalent to knowing the velocity and force in every element of the original mechanical system. The real advantage of the method resides in the application of the countless theorems and laws developed over the years in network analysis. For example, the dimensional reduction of the circuit can be realized using Thevenin/Norton theorem.

III. ELECTROMECHANICAL ANALOGUE OF A HALF-CAR MODEL BASED ON ELECTROSTATIC CAPACITOR COUPLING

In this section, the analogy is applied to a more complex mechanical system like the classical half car vehicle model depicted in figure 3, showing elastic and inertial coupling. The equations of motion of such a system could be written without inertial coupling terms if the vertical displacement of the center of mass and the pitch angle are taken as coordinates. Nevertheless, to have only translational coordinates, which facilitates the application of the electromechanical analogy, the vertical displacements of the mainframe points where the suspensions are attached, x_a and x_b, are used as coordinates. In this way, neither the mass nor the stiffness matrices are diagonal and, therefore, the system shows inertial and elastic coupling.

The mechanical system in figure 3 has four degrees of freedom. The coordinate vector is written as

$$\boldsymbol{x} = \begin{bmatrix} x_a & x_b & x_d & x_t \end{bmatrix}^T \tag{12}$$

where x_d and x_t are the vertical displacements of the unsprung masses. The equations of motion will be obtained again by using Lagrange Eq. (1) for which we need to calculate the kinetic and potential energies as well as the Rayleigh

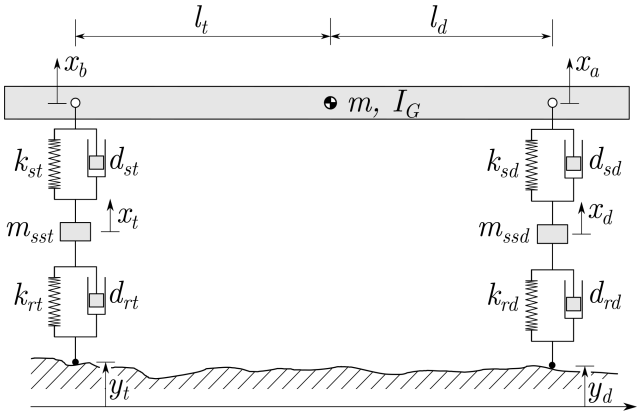

FIGURE 3. Half-car vehicle model for vertical dynamics analysis.

dissipation function as follows:

$$
\begin{aligned}
T &= \frac{m_{ssd}\dot{x}_d^2}{2} + \frac{m_{sst}\dot{x}_t^2}{2} + \frac{I_G(\dot{x}_a-\dot{x}_b)^2}{2(l_d+l_t)^2} + \frac{m(l_d\dot{x}_b+l_t\dot{x}_a)^2}{2(l_d+l_t)^2}\\
\Pi &= \frac{k_{sd}(x_a-x_d)^2}{2} + \frac{k_{st}(x_b-x_t)^2}{2} + \frac{k_{rd}(x_d-y_d)^2}{2}\\
&\quad + \frac{k_{rt}(x_t-y_t)^2}{2} + gm_{ssd}x_d + gm_{sst}x_t\\
&\quad + \frac{gm\,(l_dx_b+l_tx_a)}{l_d+l_t}\\
F_R &= \frac{d_{sd}\,(\dot{x}_a-\dot{x}_d)^2}{2} + \frac{d_{st}(\dot{x}_b-\dot{x}_t)^2}{2} + \frac{d_{rd}(\dot{x}_d-\dot{y}_d)^2}{2}\\
&\quad + \frac{d_{rt}\,(\dot{x}_t-\dot{y}_t)^2}{2}
\end{aligned}
$$

where m and I_G are the mass and moment of inertia of the vehicle frame, m_{ssd} and m_{sst} are the front and rear unsprung masses, k_{sd}, d_{sd}, k_{st}, d_{st} are the stiffness and damping constants of the front and rear suspension elements, k_{rd}, d_{rd}, k_{rt}, d_{rt} are the front and rear tyre stiffness and damping constants and y_d and y_t are the front and rear displacements of the wheel and ground contact points. Resorting to Eq. (6), the mass, damping, and stiffness matrices read as follows:

$$
\boldsymbol{m} = \begin{bmatrix}
\frac{m\,l_t{}^2+I_G}{(l_d+l_t)^2} & \frac{l_d\,l_t\,m-I_G}{(l_d+l_t)^2} & 0 & 0\\
\frac{l_d\,l_t\,m-I_G}{(l_d+l_t)^2} & \frac{m\,l_d{}^2+I_G}{(l_d+l_t)^2} & 0 & 0\\
0 & 0 & m_{ssd} & 0\\
0 & 0 & 0 & m_{sst}
\end{bmatrix}, \quad (13)
$$

$$
\boldsymbol{d} = \begin{bmatrix}
d_{sd} & 0 & -d_{sd} & 0\\
0 & d_{st} & 0 & -d_{st}\\
-d_{sd} & 0 & d_{rd}+d_{sd} & 0\\
0 & -d_{st} & 0 & d_{rt}+d_{st}
\end{bmatrix}, \quad (14)
$$

$$
\boldsymbol{k} = \begin{bmatrix}
k_{sd} & 0 & -k_{sd} & 0\\
0 & k_{st} & 0 & -k_{st}\\
-k_{sd} & 0 & k_{rd}+k_{sd} & 0\\
0 & -k_{st} & 0 & k_{rt}+k_{st}
\end{bmatrix}, \quad (15)
$$

and the generalized force vector is written as follows

$$
\boldsymbol{Q}(t) = \begin{bmatrix}
-\frac{g\,l_t\,m}{l_d+l_t}\\
-\frac{g\,l_d\,m}{l_d+l_t}\\
-g\,m_{ssd}\\
-g\,m_{sst}
\end{bmatrix} + \begin{bmatrix}
0\\
0\\
d_{rd}\,\dot{y}_d(t)+k_{rd}\,y_d(t)\\
d_{rt}\,\dot{y}_t(t)+k_{rt}\,y_t(t)
\end{bmatrix} \quad (16)
$$

where $\boldsymbol{Q}(t)$ is the sum of a gravitational force vector and a nonconstant vector dependent on the road profile. For harmonic steady-state analysis, gravitational forces can be omitted as they result in an offset that may be added if needed.

$$
\begin{bmatrix}
\vec{Y}_{11} & -C_M\omega j & -b_{sd}-\frac{1}{L_{sd}\omega j} & 0\\
-C_M\omega j & \vec{Y}_{22} & 0 & -G_{st}-\frac{1}{L_{st}\omega j}\\
-G_{sd}-\frac{1}{L_{sd}\omega j} & 0 & \vec{Y}_{33} & 0\\
0 & -G_{st}-\frac{1}{L_{st}\omega j} & 0 & \vec{Y}_{44}
\end{bmatrix}
\times \begin{bmatrix}
\vec{U}_a\\ \vec{U}_b\\ \vec{U}_d\\ \vec{U}_t
\end{bmatrix} = \begin{bmatrix}
0\\ 0\\ \vec{I}_d\\ \vec{I}_t
\end{bmatrix} \quad (17)
$$

By inspecting Eq. (13), it can be noticed that nonzero terms appear outside the diagonal. Based on circuit analysis techniques, it follows that there is an electrical coupling between variables $\ddot{\phi}_1$ and $\ddot{\phi}_2$, i.e., $\dot{u}_1$ and $\dot{u}_2$. Since we are using a force-current analogy, the right electrical analogue is depicted in figure 4. Note that the same naming convention has been retained for nodes. It can be observed that this analogue is very similar to that in figure 2b using the analogue twice but introducing a new mechanism based on electrostatic coupling between capacitors. Furthermore, note that the current source (force $f(t)$) has been removed and both, a new voltage source (to model the vertical velocity that causes the road profile) and an electrostatic capacitor coupling (to model the inertial coupling), have been included. The dots near the capacitors C_A and C_B in figure 4 indicate the polarity of the capacitor coupling. Interestingly enough, this analogue is widely used in power electronics for different applications such as electric vehicle charging [44]. Note that the use of the force-current analogy leads to a dual of the classic magnetic coupling widely used for transformers and transducers.

The circuit in figure 4 can be simplified. The coupling capacitors can be replaced [45] by two different electrical models: voltage-controlled current sources (VCCS) or capacitors arranged in Π network. Figure 5 shows the layout for both configurations and figure 6 shows the simplified circuit using the Π network. The values of the inductors and resistors follows the rules on table 1, while the values of the coupling capacitors are $C_A = \frac{ml_t{}^2+I_G}{l^2}$ and $C_B = \frac{ml_d{}^2+I_G}{l^2}$ and the coupling coefficient is $C_M = \frac{I_G-l_dl_tm}{l^2}$ as reflected in (13). To facilitate the resolution by applying KCL for a steady-state harmonic analysis, the real voltage sources have been transformed into real current sources i_t and i_d. This is one of the main benefits of using the electromechanical analogy: a plethora of rules, theorems, and laws can be

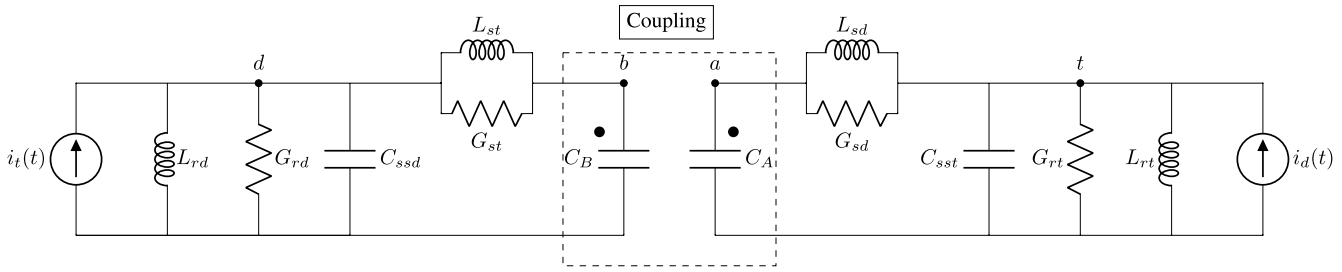

FIGURE 4. Electrical analogue of the half-car vehicle model in figure 3. The vertical velocity of each wheel is modeled through voltages sources. The inertial coupling can be modeled through an electrostatic capacitor coupling.

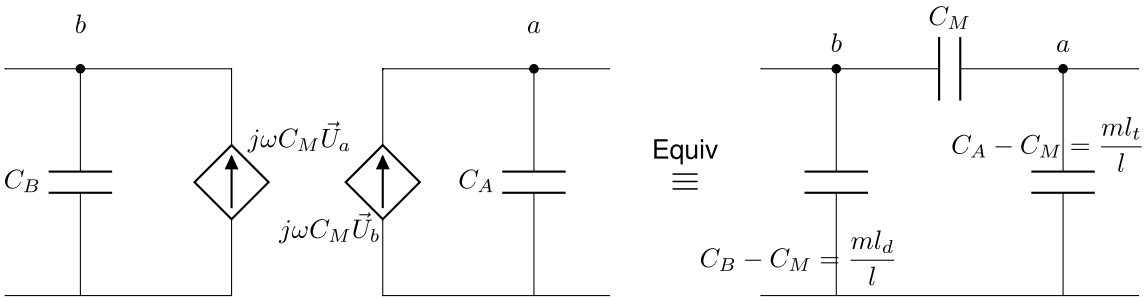

FIGURE 5. Equivalent networks for capacitive coupling. Left, voltage controlled current sources model and right, Π-network model.

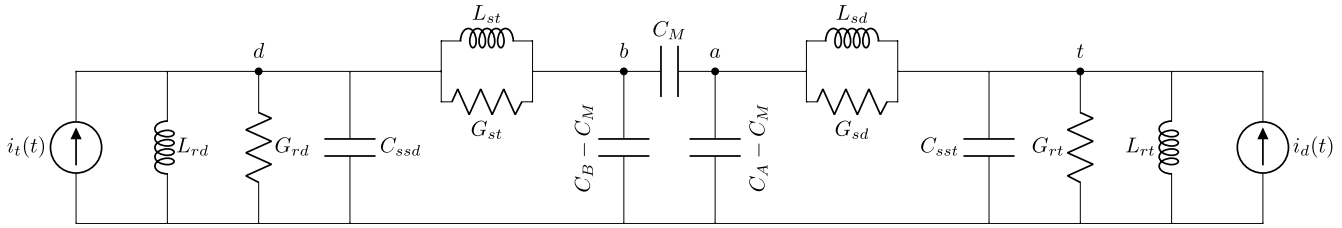

FIGURE 6. Equivalent circuit for half-car using Π-network model.

applied to simplify the proposed circuits. Note also that, from a practice point of view, a large number of computational methods and optimization algorithms developed for electrical engineering problems can be used. The resulting matrix equation is shown in (17). where

$$\begin{aligned}
\vec{Y}_{11} &= G_{sd} + C_A\omega j + \frac{1}{L_{sd}\omega j} \\
\vec{Y}_{22} &= G_{st} + C_B\omega j + \frac{1}{L_{st}\omega j} \\
\vec{Y}_{33} &= C_{ssd}\omega j + G_{sd} + G_{rd} + \frac{1}{L_{sd}\omega j} + \frac{1}{L_{rd}\omega j} \\
\vec{Y}_{44} &= C_{sst}\omega j + G_{st} + G_{rt} + \frac{1}{L_{st}\omega j} + \frac{1}{L_{rt}\omega j} \\
\vec{I}_d &= G_{rd}\vec{V}_d + \frac{1}{L_{rd}\omega j}\vec{V}_d \\
\vec{I}_t &= G_{rt}\vec{V}_t + \frac{1}{L_{rt}\omega j}\vec{V}_t
\end{aligned}$$

Note again, that gravitational forces (equivalent to DC sources) have been omitted for harmonic analysis. The terms $\vec{V}_d$ and $\vec{V}_t$ represent the voltage source analogue to the velocity of each unsprung mass caused by the road profile. Also note that in frequency domain $\frac{d}{dt} = j\omega$ and $\int dt = \frac{1}{j\omega}$. It can be observed that mechanical Eqs. (13)-(16) are the time domain analogue version of the electrical frequency domain equations in (17).

IV. APPLICATION TO A VEHICLE MODEL WITH A HIGHER LEVEL OF COMPLEXITY

In this section, the system to be analysed is a three-axle vehicle model, which has interest because the vertical displacement of the attachment point of the middle axle, x_c, is dependent on x_a and x_b. In other words, x_c is a dependent coordinate which is written in terms of x_a and x_b as follows

$$x_c = (l_b\, x_a - l_b\, x_b + l_d\, x_b + l_t\, x_b)\, /l \tag{18}$$

where distances l_a, l_b, l_d and l_t are defined in figure 7. To keep the text of the manuscript to a reasonable size, the reader is referred to figure 7 to find the meaning of the mass, damping, and stiffness constants of this system.

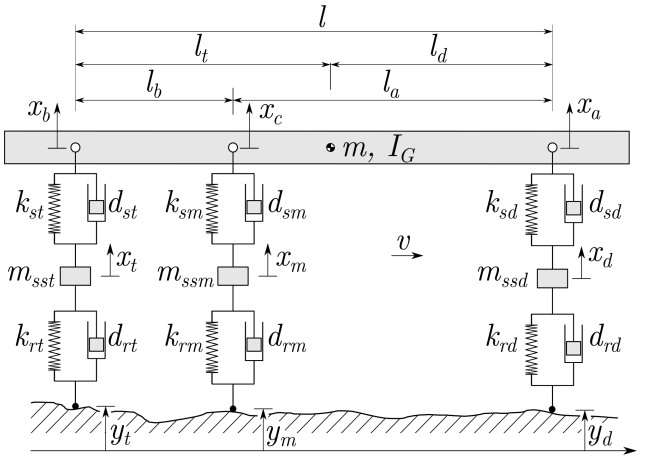

FIGURE 7. Three-axle vehicle model for vertical dynamics analysis.

This system is modeled in terms of the following coordinate vector

$$\boldsymbol{x} = \begin{bmatrix} x_a & x_b & x_d & x_t & x_m \end{bmatrix}^T \tag{19}$$

It can be demonstrated with the help of Lagrange equations that the mass, damping, and stiffness matrices, according to Eq. (6), are written as follows

$$\boldsymbol{m} = \begin{bmatrix} m_{11} & m_{12} & 0 & 0 & 0 \\ m_{21} & m_{22} & 0 & 0 & 0 \\ 0 & 0 & m_{ssd} & 0 & 0 \\ 0 & 0 & 0 & m_{sst} & 0 \\ 0 & 0 & 0 & 0 & m_{ssm} \end{bmatrix} \tag{20}$$

where $m_{11} = \left(m{l_t}^2 + I_G\right)/l^2$, $m_{22} = \left(m\,{l_d}^2 + I_G\right)/l^2$, and $m_{12} = m_{12} = \left(-I_G + l_d\, l_t\, m\right)/l^2$.

$$\boldsymbol{d} = \begin{bmatrix} d_{11} & d_{12} & -d_{sd} & 0 & d_{15} \\ d_{21} & d_{22} & 0 & -d_{st} & d_{25} \\ -d_{sd} & 0 & d_{rd} + d_{sd} & 0 & 0 \\ 0 & -d_{st} & 0 & d_{rt} + d_{st} & 0 \\ d_{51} & d_{52} & 0 & 0 & d_{rm} + d_{sm} \end{bmatrix} \tag{21}$$

where $d_{11} = d_{sd} + d_{sm}\,{l_b}^2/l^2$, $d_{12} = d_{21} = d_{sm}\,l_a\,l_b/l^2$, $d_{15} = d_{51} = -d_{sm}\,l_b/l$, $d_{22} = d_{st} + d_{sm}\,{l_a}^2/l^2$ and $d_{25} = d_{52} = -d_{sm}\,l_a/l$.

$$\boldsymbol{k} = \begin{bmatrix} k_{11} & k_{12} & -k_{sd} & 0 & k_{15} \\ k_{21} & k_{22} & 0 & -k_{st} & k_{25} \\ -k_{sd} & 0 & k_{rd} + k_{sd} & 0 & 0 \\ 0 & -k_{st} & 0 & k_{rt} + k_{st} & 0 \\ k_{51} & k_{52} & 0 & 0 & k_{rm} + k_{sm} \end{bmatrix} \tag{22}$$

where $k_{11} = k_{sd} + k_{sm}\,{l_b}^2/l^2$, $k_{12} = k_{21} = k_{sm}\,l_a\,l_b/l^2$, $k_{15} = k_{51} = -k_{sm}\,l_b/l$, $k_{22} = k_{st} + k_{sm}\,{l_a}^2/l^2$ and $k_{25} = k_{52} = -k_{sm}\,l_a/l$.

The generalized force vector is written as follows:

$$\boldsymbol{Q}(t) = \begin{bmatrix} -\dfrac{g\,l_t\,m}{l} \\ -\dfrac{g\,l_d\,m}{l} \\ -g\,m_{ssd} \\ -g\,m_{sst} \\ -g\,m_{ssm} \end{bmatrix} + \begin{bmatrix} 0 \\ 0 \\ d_{rd}\,\dot{y}_d(t) + k_{rd}\,y_d(t) \\ d_{rt}\,\dot{y}_t(t) + k_{rt}\,y_t(t) \\ d_{rm}\,\dot{y}_m(t) + k_{rm}\,y_m(t) \end{bmatrix} \tag{23}$$

where y_d, y_m and y_t are the front, middle and rear vertical displacements of the wheel and ground contact points. It should be noted that matrix (20) is very similar to (13) but with a new element in the diagonal that accounts for the mass m_{ssm}. However, matrix equations (21) and (22) differ to those of a half-car. Now, new elements arise in positions 12 (and symmetrically in 21). In addition, elements 11 and 22 change their value. The equivalent electrical model is shown in figure 8. As a result, the half-car model is extended by adding a new node, m, (due to the new axle) with new elements connecting node a and b with m. Moreover, a new branch connecting a and b is observed. Interestingly enough, this branch has elements with negative values. Finally, the node m is linked to ground through the expected elements in a similar fashion as the other two wheels. The road profile of the third wheel is modeled through a new voltage source v_m.

The new matrix equation reads as follows:

$$\begin{bmatrix} \vec{Y}_{11} & \vec{Y}_{12} & \vec{Y}_{13} & 0 & \vec{Y}_{15} \\ \vec{Y}_{21} & \vec{Y}_{22} & 0 & \vec{Y}_{24} & \vec{Y}_{25} \\ \vec{Y}_{31} & 0 & \vec{Y}_{33} & 0 & 0 \\ 0 & \vec{Y}_{42} & 0 & \vec{Y}_{44} & 0 \\ \vec{Y}_{51} & \vec{Y}_{52} & 0 & 0 & \vec{Y}_{55} \end{bmatrix} \begin{bmatrix} \vec{U}_a \\ \vec{U}_b \\ \vec{U}_d \\ \vec{U}_t \\ \vec{U}_m \end{bmatrix} = \begin{bmatrix} 0 \\ 0 \\ \vec{I}_d \\ \vec{I}_t \\ \vec{I}_m \end{bmatrix} \tag{24}$$

where

$$\vec{Y}_{11} = G_{sd} + C_A\omega j + \frac{1}{L_{sd}\omega j} + \left(G_{sm} + \frac{1}{L_{sm}\omega j}\right)\frac{l_b^2}{l^2}$$

$$\vec{Y}_{22} = G_{st} + C_B\omega j + \frac{1}{L_{st}\omega j} + \left(G_{sm} + \frac{1}{L_{sm}\omega j}\right)\frac{l_a^2}{l^2}$$

$$\vec{Y}_{33} = C_{ssd}\omega j + G_{sd} + G_{rd} + \frac{1}{L_{sd}\omega j} + \frac{1}{L_{rd}\omega j}$$

$$\vec{Y}_{44} = C_{sst}\omega j + G_{st} + G_{rt} + \frac{1}{L_{st}\omega j} + \frac{1}{L_{rt}\omega j}$$

$$\vec{Y}_{55} = C_{ssm}\omega j + G_{sm} + G_{rm} + \frac{1}{L_{sm}\omega j} + \frac{1}{L_{rm}\omega j}$$

$$\vec{Y}_{12} = \vec{Y}_{21} = -C_M\omega j + \left(G_{sm} + \frac{1}{L_{sm}\omega j}\right)\frac{l_a l_b}{l^2}$$

$$\vec{Y}_{13} = \vec{Y}_{31} - b_{sd} - \frac{1}{L_{sd}\omega j}$$

$$\vec{Y}_{15} = \vec{Y}_{51} = -\left(G_{sm} + \frac{1}{L_{sm}\omega j}\right)\frac{l_b}{l}$$

$$\vec{Y}_{24} = \vec{Y}_{42} = -G_{st} - \frac{1}{L_{st}\omega j}$$

$$\vec{Y}_{25} = \vec{Y}_{52} = -\left(G_{sm} + \frac{1}{L_{sm}\omega j}\right)\frac{l_a}{l}$$

TABLE 2. Constants of the lumped parameter three axle vehicle model.

Parameter	Symbol	Value	Units
mass	m	22,000	kg
pitch moment of inertia	I_G	21,000	kgm^2
front axle unsprung mass	m_{ssd}	900	kg
middle axle unsprung mass	m_{ssm}	1,400	kg
rear axle unsprung mass	m_{sst}	1,400	kg
front axle suspension stiffness	k_{sd}	610,000	N/m
middle axle suspension stiffness	k_{sm}	2,600,000	N/m
rear axle suspension stiffness	k_{st}	2,600,000	N/m
front axle suspension damping	d_{sd}	15,400	Ns/m
middle axle suspension damping	d_{sm}	15,400	Ns/m
rear axle suspension damping	d_{st}	15,400	Ns/m
front axle tyre stiffness	k_{rd}	1,360,000	N/m
middle axle tyre stiffness	k_{rm}	5,430,000	N/m
rear axle tyre stiffness	k_{rt}	5,430,000	N/m
front axle tyre damping	d_{rd}	150	Ns/m
middle axle tyre damping	d_{rm}	150	Ns/m
rear axle tyre damping	d_{rt}	150	Ns/m
rear to front axle distance	l	6.15	m
truck center of mass to front axle distance	l_d	4.44	m
truck center of mass to rear axle distance	l_t	1.71	m
middle to front axle distance	l_a	4.80	m
middle to rear axle distance	l_b	1.35	m

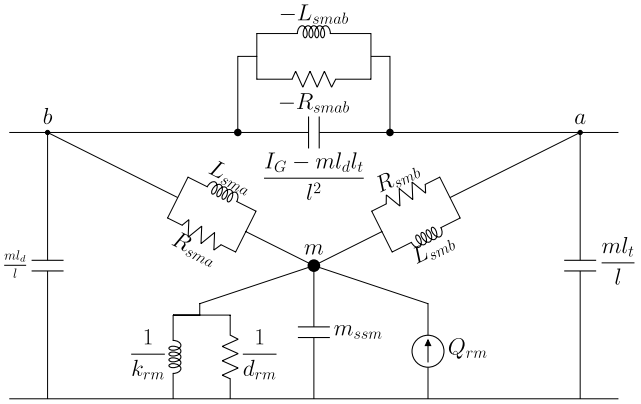

FIGURE 8. Electrical analogue of the three-axle vehicle model (zoomed in the coupling area of figure 6). $L_{sma} = \frac{l}{k_{sm}l_a}$, $L_{smb} = \frac{l}{k_{sm}l_b}$, $R_{sma} = \frac{l}{R_{sm}l_a}$, $R_{smb} = \frac{l}{k_{sm}l_b}$, $L_{smab} = \frac{l}{k_{sm}l_al_b}$ and $R_{smab} = \frac{l}{R_{sm}l_al_b}$.

$$\vec{I}_d = G_{rd}\vec{V}_d + \frac{1}{L_{rd}\omega j}\vec{V}_d, \quad \vec{I}_t = G_{rt}\vec{V}_t + \frac{1}{L_{rt}\omega j}\vec{V}_t$$
$$\vec{I}_m = G_{rm}\vec{V}_m + \frac{1}{L_{rm}\omega j}\vec{V}_m$$

V. NUMERICAL RESULTS. VALIDATION OF ELECTROMECHANICAL ANALOGUES

To show the benefits of the presented analogy, a numerical example of an electrical analogue of a three-axle vehicle model in steady-state harmonic vibration is solved. The model is inspired by the real three-axle heavy truck modeled by Wang *et al.* [46]. The constants of the lumped parameter truck model are summarized in Table 2.

The vehicle model is assumed to travel at a constant forward velocity, $v = 60$ km/h, on a road with a harmonic unevenness characterized by amplitude, $Y = 5$ cm and a wavelength, $\lambda = 2$ m. This way, the displacements of the front, middle, and rear tyre-ground contact points can be modeled as follows:

$$\begin{aligned} y_d(t) &= Y \sin(2\pi vt/\lambda) \\ y_m(t) &= Y \sin(2\pi vt/\lambda - \phi_m) \\ y_t(t) &= Y \sin(2\pi vt/\lambda - \phi_t) \end{aligned} \tag{25}$$

where $\phi_m = 2\pi l_a/\lambda$ and $\phi_t = 2\pi l/\lambda$ are phase shifts.

To solve the electrical analogue in harmonic steady state analysis, we must first perform the complex phasor representation of the variables presented in table 2 and then insert them into Eq. (24) to solve the linear matrix system. Table 3 shows the complex phasor values of elements in (24) for this example. The vector current is also presented in complex form. The unknowns $\vec{U} = [\vec{U}_a, \vec{U}_b, \vec{U}_d, \vec{U}_t, \vec{U}_m]^T$ are easily obtained by performing the inverse of the admittance matrix and then multiply the current vector $\vec{I}$. The result is

$$\begin{bmatrix} \vec{U}_a \\ \vec{U}_b \\ \vec{U}_d \\ \vec{U}_t \\ \vec{U}_m \end{bmatrix} = \begin{bmatrix} 0.0754 + 0.5293i \\ -0.0987 + 0.0033i \\ -0.8114 - 2.1287i \\ 1.7945 - 1.4511i \\ -2.1784 - 0.9272i \end{bmatrix} = \begin{bmatrix} 0.5346 \times e^{81.90\ i} \\ 0.0988 \times e^{178.11\ i} \\ 2.2781 \times e^{-110.87\ i} \\ 2.3078 \times e^{-38.96\ i} \\ 2.3675 \times e^{-156.94\ i} \end{bmatrix} \tag{26}$$

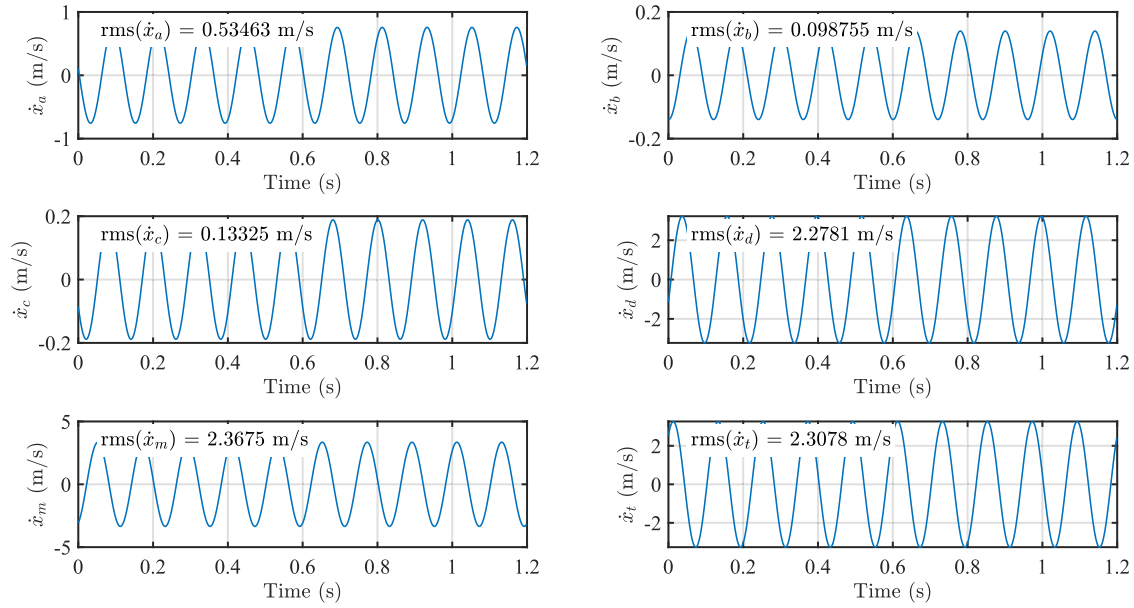

FIGURE 9. Steady state vertical oscillation velocities of the characteristic points (*a*, *b*, *c*, *d*, *m*, and *t*) of the three-axle vehicle model.

TABLE 3. Complex phasor data in (24) for 3-axle numerical example. All values are multiplied by 10^{-5}.

		1	2	3	4	5
$[\vec{Y}]$ matrix	1	0.1614 + 1.0408j	0.0264 + 1.9365j	-0.1540 + 0.1165j	0	-0.0338 + 0.1090j
	2	0.0264 + 1.9365j	0.2478 + 5.4956j	0	-0.1540 + 0.4966j	-0.1202 + 0.3876j
	3	-0.1540 + 0.1165j	0	0.1555 + 0.0950j	0	0
	4	0	-0.1540 + 0.4966j	0	0.1555 − 0.8006j	0
	5	-0.0338 + 0.1090j	-0.1202 + 0.3876j	0	0	0.1555 − 0.8006j
	$\vec{I}$	0	0	0.0028 - 0.4808j	-0.8691 - 1.7118j	-1.1307 + 1.5515j

The result in (26) are complex values representing the voltage (velocities) in the electrical (mechanical) circuit. The norm of the complex phasor gives the RMS amplitude for each harmonic sinusoidal waveform. The time-domain expressions are

$$\begin{aligned} u_a(t) &= \sqrt{2}\,0.5346\sin(\omega t + 81.90) \\ u_b(t) &= \sqrt{2}\,0.0988\sin(\omega t + 178.11) \\ u_d(t) &= \sqrt{2}\,2.2781\sin(\omega t - 110.87) \\ u_t(t) &= \sqrt{2}\,2.3078\sin(\omega t - 38.96) \\ u_m(t) &= \sqrt{2}\,2.3675\sin(\omega t - 156.94) \end{aligned} \tag{27}$$

in Volt (meter/second) for the electrical (mechanical) circuit. The phase angle is expressed in degrees.

To validate the previous results, the steady-state harmonic vibration of the three-axle vehicle model is studied with the help of the inverse Fourier transform. As it is well known, the steady-state oscillation velocity vector can be obtained as follows:

$$\dot{\boldsymbol{x}}(t) = \int_{-\infty}^{\infty} j\omega \boldsymbol{H}(\omega)\boldsymbol{Q_h}(\omega)\mathrm{e}^{j\omega t}\,\mathrm{d}\omega \tag{28}$$

where $\boldsymbol{H}(\omega) = \left(-\omega^2\boldsymbol{m} + j\omega\boldsymbol{d} + \boldsymbol{k}\right)^{-1}$ is the frequency response matrix function and $\boldsymbol{Q_h}(\omega)$ is the Fourier transform of the harmonic part of the excitation, which is obtained as follows

$$\boldsymbol{Q_h}(\omega) = \frac{1}{2\pi}\int_{-\infty}^{\infty} \begin{bmatrix} 0 \\ 0 \\ d_{rd}\,\dot{y}_d(t) + k_{rd}\,y_d(t) \\ d_{rt}\,\dot{y}_t(t) + k_{rt}\,y_t(t) \\ d_{rm}\,\dot{y}_m(t) + k_{rm}\,y_m(t) \end{bmatrix} \mathrm{e}^{-j\omega t}\,\mathrm{d}t \tag{29}$$

Note that the constant part of the excitation vector appearing in Eq. (23) has been ignored for this analysis since it does not affect the velocity in steady-state. The velocities in Eq. (28) have been solved with the help of the `ifft` subroutine, while $\boldsymbol{Q_h}(\omega)$ is computed with the `fft` subroutine, both from Matlab. For the solution, a total of ten oscillations with 1024 time points have been simulated. This gave a sampling frequency of 833.33 Hz, for an excitation frequency of 8.33 Hz. Finally, the velocity $\dot{x}_c(t)$ is obtained from the velocities of points a and b as follows:

$$\dot{x}_c = \left(l_b\,\dot{x}_a - l_b\,\dot{x}_b + l_d\,\dot{x}_b + l_t\,\dot{x}_b\right)/l \tag{30}$$

The velocities obtained for the characteristic points (a, b, c, d, m, and t) of the three-axle vehicle model are shown in Figure 9 together with the RMS values of the velocity signals for comparison against the results of Eq. (27). As it can be seen, the RMS values exactly coincide with those of the electrical analogue circuit.

VI. SUMMARY AND CONCLUSION

The use of electrical analogues of vehicle models is a topic of interest and has been studied previously in the literature. In particular, the quarter car model has been studied in several publications. Such electrical analogues have been successfully used for tuning controllers of active suspension elements. Nevertheless, more complex models, such as the half-car vehicle model, lack a comprehensive electrical analogue. This work attempts to shed some light on this subject by providing the electrical analogue of the half-car model as well as its closely related, but more complicated model, three-axle vehicle. Therefore, new and non-previously disclosed electrical analogues for two moderately complex vehicle models have been described.

The inertial coupling present in such mechanical systems due to the vehicle mainframe has been identified and modeled for the first time by an electrostatic capacitor coupling in its force-current analogue. Only pure displacement coordinates have been used instead of mixing angle and displacement variables. The capacitance values of the coupled capacitors depend on the mass and moment of inertia of the vehicle mainframe, and the distance of each wheel to the center of gravity of the mainframe. To deal with the coupling capacitors, its equivalent Π network has been used to simplify the resulting equations. The transformation between real voltage and current sources has been also used to facilitate the application of KCL's.

Finally, numerical results have been obtained for a three-axle vehicle model in steady-state harmonic vibration conditions both by using the electrical equivalent circuit and the mechanical model as an example of the utility of this method. As expected, both approaches led to the same results by sharing the same time and frequency domain equations.

The presented methodology would be of interest for further studies where coupled electrical and mechanical systems are available. The design of control strategies of active suspension systems is a classic example. Furthermore, the proposed analogy opens up new possibilities for the application of some well-known tools in Circuit Theory analysis.

REFERENCES

[1] D. Jeltsema and J. M. Scherpen, "Multidomain modeling of nonlinear networks and systems," *IEEE Control Syst. Mag.*, vol. 29, no. 4, pp. 28–59, 2009.

[2] F. A. Firestone, "A new analogy between mechanical and electrical systems," *J. Acoust. Soc. Amer.*, vol. 4, no. 3, pp. 249–267, Jan. 1933.

[3] H. Olson, *Dynamical Analogies*. New York, NY, USA: Van Nostrand Company, 1943.

[4] A. Bloch, "Electromechanical analogies and their use for the analysis of mechanical and electromechanical systems," *J. Inst. Electr. Eng. I, Gen.*, vol. 92, no. 52, pp. 157–169, Apr. 1945.

[5] W. P. Mason, "Electrical and mechanical analogies," *Bell System Tech. J., The*, vol. 20, no. 4, pp. 405–414, Oct. 1941.

[6] J. Miles, "Applications and limitations of mechanical-electrical analogies, new and old," *J. Acoust. Soc. Amer.*, vol. 14, no. 3, pp. 183–192, Jan. 1943.

[7] H. C. Harrison, "Acoustic device," U.S. Patent 1 730 425, Oct. 8, 1929.

[8] P. Gardonio and M. J. Brennan, "On the origins and development of mobility and impedance methods in structural dynamics," *J. Sound Vibrat.*, vol. 249, no. 3, pp. 557–573, Jan. 2002.

[9] W. Hähnle, "Die darstellung elektromechanischer gebilde durch rein elektrische schaltbilder," in *Wissenschaftliche Veröffentlichungen aus dem Siemens-Konzern*. Berlin, Germany: Springer, 1932, pp. 1–23.

[10] F. A. Firestone, "The mobility method of computing the vibration of linear mechanical and acoustical systems: Mechanical-electrical analogies," *J. Appl. Phys.*, vol. 9, no. 6, pp. 373–387, Jun. 1938.

[11] B. B. Bauer, "Transformer couplings for equivalent network synthesis," *J. Acoust. Soc. Amer.*, vol. 25, no. 5, pp. 837–840, Sep. 1953.

[12] P. Le Corbeiller and Y.-W. Yeung, "Duality in mechanics," *J. Acoust. Soc. Amer.*, vol. 24, no. 6, pp. 643–648, 1952.

[13] P. Gardonio and M. J. Brennan, "Mobility and impedance methods in structural dynamics: An historical review," ISVR, Southampton, U.K., ISVR Tech. Rep. 289, 2000. [Online]. Available: https://eprints.soton.ac.uk/10794/1/Pub1041.pdf

[14] A. Falaize and T. Hélie, "Passive modelling of the electrodynamic loudspeaker: From the Thiele–Small model to nonlinear port-Hamiltonian systems," *Acta Acustica*, vol. 4, no. 1, p. 1, 2020.

[15] N. Tiwari, A. Puri, and A. Saraswat, "Lumped parameter modelling and methodology for extraction of model parameters for an electrodynamic shaker," *J. Low Freq. Noise, Vibrat. Act. Control*, vol. 36, no. 2, pp. 99–115, Jun. 2017.

[16] C. W. de Silva, "Use of linear graphs and Thevenin/Norton equivalent circuits in the modeling and analysis of electro-mechanical systems," *Int. J. Mech. Eng. Educ.*, vol. 38, no. 3, pp. 204–232, Jul. 2010.

[17] C. W. D. Silva, *Modeling of Dynamic Systems With Engineering Applications*. Boca Raton, FL, USA: CRC Press, 2017.

[18] R. Plunkett, *Colloquium on Mechanical Impedance Methods for Mechanical Vibrations: Presented at the ASME Annual Meeting, New York, NY, December 2, 1958*. New York, NY, USA: American Society of Mechanical Engineers, 1958.

[19] C. W. de Silva, "A systematic approach for modeling multi-physics systems," *Int. J. Mech. Eng. Educ.*, vol. 49, no. 2, pp. 122–150, 2019.

[20] R. C. Bergvall and P. H. Robinson, "Quantitative mechanical analysis of power system transient disturbances," *Trans. Amer. Inst. Electr. Eng.*, vol. 47, no. 3, pp. 915–925, Jul. 1928.

[21] H. J. Reich, "A mechanical analogy for coupled electrical circuits," *Rev. Sci. Instrum.*, vol. 3, no. 6, pp. 287–293, Jun. 1932.

[22] M. Pawley, "The design of a mechanical analogy for the general linear electrical network with lumped parameters," *J. Franklin Inst.*, vol. 223, no. 2, pp. 179–198, Feb. 1937.

[23] L. O. Chua, "Memristor-the missing circuit element," *IEEE Trans. Circuit Theory*, vol. CT-18, no. 5, pp. 507–519, Sep. 1971.

[24] D. B. Strukov, G. S. Snider, D. R. Stewart, and R. S. Williams, "The missing memristor found," *Nature*, vol. 453, pp. 80–83, May 2008.

[25] G. F. Oster and D. M. Auslander, "The memristor: A new bond graph element," *J. Dyn. Syst., Meas., Control*, vol. 94, no. 3, pp. 249–252, Sep. 1972, doi: 10.1115/1.3426595.

[26] M. C. Smith, "Synthesis of mechanical networks: The inerter," *IEEE Trans. Autom. Control*, vol. 47, no. 10, pp. 1648–1662, Oct. 2002.

[27] X. Yang, L. Yan, Y. Shen, Y. Liu, and C. Liu, "Optimal design and dynamic control of an ISD vehicle suspension based on an ADD positive real network," *IEEE Access*, vol. 8, pp. 94294–94306, 2020.

[28] J. Nie, Y. Yang, T. Jiang, and H. Zhang, "Passive skyhook suspension reduction for improvement of ride comfort in an off-road vehicle," *IEEE Access*, vol. 7, pp. 150710–150719, 2019.

[29] F. Pehlivan, C. Mizrak, and I. Esen, "Modeling and validation of 2-DOF rail vehicle model based on electro–mechanical analogy theory using theoretical and experimental methods," *Eng., Technol. Appl. Sci. Res.*, vol. 8, no. 6, pp. 3603–3608, Dec. 2018.

[30] X. Xu, H. Jiang, and M. H. Gao, "Modeling and validation of air suspension with auxiliary chamber based on electromechanical analogy theory," *Appl. Mech. Mater.*, vol. 437, pp. 190–193, Oct. 2013.

[31] N. Jiamei, Z. Xiaoliang, and C. Long, "Suspension employing inerter and optimization based on vibration isolation theory on electrical-mechanical analogies," in *Proc. Int. Conf. Optoelectron. Image Process.*, Nov. 2010, pp. 481–484.

[32] Y. Shen, Y. Liu, L. Chen, and X. Yang, "Optimal design and experimental research of vehicle suspension based on a hydraulic electric inerter," *Mechatronics*, vol. 61, pp. 12–19, Aug. 2019.
[33] J. Y. Routex, S. Gay-Desharnais, and M. Ehsani, "Study of hybrid electric vehicle drive train dynamics using gyrator-based equivalent circuit modeling," SAE, Warrendale, PA, USA, Tech. Rep. 2002-01-1083, 2002.
[34] F. Fahy and J. Walker, *Advanced Applications in Acoustics, Noise and Vibration*. Boca Raton, FL, USA: CRC Press, 2018.
[35] L. G. Lenning, A. Shah, U. Ozguner, and S. B. Bibyk, "Integration of VLSI circuits and mechanics for vibration control of flexible structures," *IEEE/ASME Trans. Mechatronics*, vol. 2, no. 1, pp. 30–40, Mar. 1997.
[36] P. Luca, A. Reatti, F. Corti, and R. A. Mastromauro, "Inductive power transfer: Through a bondgraph analogy, an innovative modal approach," in *Proc. IEEE Int. Conf. Environ. Electr. Eng. IEEE Ind. Commercial Power Syst. Eur. (EEEIC/I&CPS Eur.)*, Jun. 2017, pp. 1–6.
[37] Y. Liao and J. Liang, "Unified modeling, analysis and comparison of piezoelectric vibration energy harvesters," *Mech. Syst. Signal Process.*, vol. 123, pp. 403–425, May 2019.
[38] B. Lossouarn, J.-F. Deü, M. Aucejo, and K. A. Cunefare, "Multimodal vibration damping of a plate by piezoelectric coupling to its analogous electrical network," *Smart Mater. Struct.*, vol. 25, no. 11, Nov. 2016, Art. no. 115042.
[39] M. R. Bai and K.-Y. Ou, "Design and implementation of electromagnetic active control actuators," *J. Vibrat. Control*, vol. 9, no. 8, pp. 997–1017, Aug. 2003.
[40] F. I. Mamedov, R. B. Dadasheva, R. A. Guseinov, A. S. Akhmedova, and N. O. Alieva, "Mathematical model of two-step vibroexciter with low mechanical frequency," *Russian Electr. Eng.*, vol. 81, no. 8, pp. 447–451, Aug. 2010.
[41] R. Mukhiya, M. Garg, P. Gaikwad, S. Sinha, A. K. Singh, and R. Gopal, "Electrical equivalent modeling of MEMS differential capacitive accelerometer," *Microelectron. J.*, vol. 99, May 2020, Art. no. 104770.
[42] Y. Qian, A. Salehian, S.-W. Han, and H.-J. Kwon, "Design and analysis of an ultrasonic tactile sensor using electro-mechanical analogy," *Ultrasonics*, vol. 105, Jul. 2020, Art. no. 106129.
[43] F. Gantmakher, *Lectures in Analytical Mechanics [by] F. Gantmacher: Translated from the Russian by George Yankovsky*. Moscow, Russia: Mir Publishers, 1970.
[44] K. Yi, "Capacitive coupling wireless power transfer with quasi-LLC resonant converter using electric vehicles' Windows," *Electronics*, vol. 9, no. 4, p. 676, Apr. 2020.
[45] H. Zhang, F. Lu, H. Hofmann, W. Liu, and C. C. Mi, "A four-plate compact capacitive coupler design and LCL-compensated topology for capacitive power transfer in electric vehicle charging application," *IEEE Trans. Power Electron.*, vol. 31, no. 12, pp. 8541–8551, Dec. 2016.
[46] W. Wang, J. Li, G. Liu, and Z. Zhang, "Simulation study on ride comfort of three-axle heavy vehicle spatial model based on rigid-elastic model and pseudo-excitation method," *J. Adv. Mech. Des., Syst., Manuf.*, vol. 14, no. 1, 2020, Art. no. JAMDSM0016.

JAVIER LÓPEZ-MARTÍNEZ received the M.S. degree in industrial engineering from the School of Industrial Engineering, University of Málaga, in 2005, and the Ph.D. degree from the University of Almería, in 2014. After some years of professional work as a Project Engineer, he began teaching at the University of Almería. He is currently an Associate Professor with the Department of Engineering. His research interest includes mechanical design, contributing with more than 15 journal articles and seven patents. He received the Ph.D. scholarship.

JAVIER CASTILLO MARTÍNEZ received the bachelor's degree in mechanical engineering from the University of Almería, in 2014, the master's degree in industrial engineering from the National University of Distance Education, in 2018, and the master's degree in occupational risk prevention from Rey Juan Carlos University, in 2018. He is currently pursuing the Ph.D. degree in technology of greenhouses and industrial engineering with the University of Almería. He began working designing machines to date, while completing his master's degrees. He began to work as an Adjunct Professor of engineering with the University of Almería, in 2019.

DANIEL GARCÍA-VALLEJO studied mechanical engineering at the University of Málaga, Spain. He received the Ph.D. degree in flexible multibody dynamics from the University of Seville, Spain, in 2006. He is currently an Associate Professor with the Department of Mechanical Engineering and Manufacturing, University of Seville, where he has taught theory of machines and mechanisms and mechanical vibrations for more than 15 years. He has more than 40 publications in journals, conferences proceedings, and book chapters. His research interests include dynamics of multibody systems, nonlinear dynamical systems, and optimal design and optimal control applied to mechanical systems.

ALFREDO ALCAYDE studied computer science engineering at the University of Almería. Spain. He received the Ph.D. degree in optimization from the University of Almería, in 2011, with a focus on electrical engineering and renewable energies using evolutionary multiobjective algorithms. He is currently a member of the Engineering Department, University of Almería, where he has spent two years researching and teaching in areas, such as power systems, energy savings, and optimization. He has published more than 20 articles in journals, conferences, and workshops, and also has several publications in books and conference proceedings.

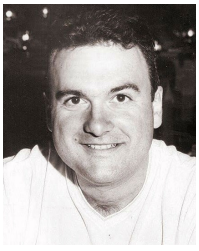

FRANCISCO G. MONTOYA studied electrical engineering at the University of Málaga, Spain. He received the Ph.D. degree in evolutionary optimization techniques applied to power systems from the University of Granada, in 2009. He is currently a member of the Engineering Department, University of Almería, where he has spent 15 years as an Associate Professor, researching and teaching in areas, such as power systems, energy savings, and optimization. He has published more than 70 articles in journals, conferences, and workshops, and has several publications in books and conference proceedings. He is one of the creators of the geometric algebra power theory applied to power systems in frequency and time domains (https://www.scopus.com/authid/detail.uri?authorId=7005663229).